Published in final edited form as:
Addit Manuf. 2018 ; 23: . doi:10.1016/j.addma.2018.08.015.

Real-time acoustic emission monitoring of powder mass flow rate for directed energy deposition

Justin Whiting[1,*], **Adam Springer**, and **Federico Sciammarella**

Department of Mechanical Engineering, Northern Illinois University, DeKalb, IL 60115, USA

[1]Engineering Laboratory, National Instituteof Standards and Technology, Gaithersburg, MD 20899, USA.

Abstract

In order to ensure a reliable and repeatable additive manufacturing process, the material delivery rate in the directed energy deposition (DED) process requires in situ monitoring and control. This paper demonstrates acoustic emission (AE) sensing as a method of monitoring the flow of powder feedstock in a powder fed DED process. With minimal calibration, this signal closely correlates to the actual mass flow rate. This article describes the fabricated mass flow monitoring system, documents various conditions in which the actual flow rate deviates from its set value, and details situations that highlight the system's utility. While AE mass flow monitoring is not free of concerns, its features make it an attractive measurement technique in the powder-fed DED process. The work presented here highlights the results obtained and illustrates that accurate monitoring of powder flow in real-time regardless of environmental conditions within the build chamber is possible.

Keywords

Acoustic emission; Directed energy deposition; Powder flow rate; Quantitative nondestructive evaluation; In situ monitoring

1. Introduction

The overall goal of this paper is to demonstrate the feasibility of creating a time series that relates a signal, the output of an acoustic emission sensor, and the mass flow rate of a stream of metallic powder In this case, the sensor detects mechanical acoustic waves. The sensor transduces the acoustic waves into an electrical signal. As is the case with any waveform, it is possible to extract various features (e.g., amplitude, frequency spectrum characteristics) from the acquired signal. These features can be used to provide information concerning a given physical phenomenon. In this example, the physical phenomenon detected is a powder mass flow rate with the root mean square (RMS) chosen as the signal feature.

While the ability to predict the powder mass flow rate is important, it is equally as important to control the powder mass flow rate in situ. This is one of the current challenges for

*Corresponding author.

powder-fed directed energy deposition (DED) impeding the technique from making its way into mainstream manufacturing processes. The powder-fed directed energy deposition process is one of the various metal additive manufacturing (AM) techniques where the deposition of powder metal occurs into a molten pool created by a high-power laser. It is possible to use various scan strategies to optimize geometries, mechanical properties, and density [1–5]. One of the earliest DED processes is known as laser engineered net shaping (LENS).[2] The LENS process typically includes four powder streams flowing through four powder delivery nozzles into the laser beam's radial center [6].

There are three primary factors which can alter the single-track characteristics and, in turn, the properties of the final part. These factors are the powder feed rate, the scanning speed, and the laser power; each of which merits consideration as they all affect the size of the melt pool. The size of the melt pool, along with other ancillary variables, dictates how quickly the melt pool solidifies, and therefore is a central factor in the AM part's final mechanical properties.

The material delivery rate largely affects the outcome of the DED process, which has been illustrated theoretically in [1,3] as well as experimentally [4,5,7–9]. An empirically verified model created by Kumar et al. [1] illustrated the geometric variations of single-track deposits caused by changes in the powder flow rate. Neela and De [3] modeled the DED process using finite element analysis and found the powder flow rate to influence the thermal behavior of deposited material and subsequently the final AM part. Ferguson et al. [4] used the LENS process to develop a semi-empirical model predicting single-track geometry as well as porosity. The research exhibited an upper limit of powder flow rate per unit length; exceeding this resulted in lack of fusion porosity. Pityana et al. [7] reported the powder flow rate positively correlates to the microhardness as well as the width and height of a deposited track. Majumdar et al. [8] identified a specific range of powder flow rate that would minimize porosity. Wang et al. [9] found the intra-layer porosity to correlate to the stability of powder flow. Research and production efforts have relied upon the powder delivery mechanism to provide a constant material delivery rate, but without a way to measure the flow, these assumptions cannot be affirmed or refuted.

While current commercial AM machines have no monitoring of the condition of the powder delivery system, there has been some research published on the topic. The limited scope of work done relies on optically based systems and on the consistency of the powder feeders. One common optical mass flow measurement method uses a laser diode directed perpendicular to the flow and a photodiode or photoelectric sensor aligned coaxially on the opposite side of the flow measuring the intensity of the emitted light [10–12]. Alternatively, a charge coupled device (CCD) camera measures the intensity of luminance, which, in theory, is proportional to the number of particles [13]. There are a few drawbacks in using this type of mass flow meter. Firstly, as the powder traveling through the sensing device is often of an abrasive nature, damage will occur to the pass-through window over time. This

[2]Certain commercial entities, equipment, or materials may be identified in this document in order to describe an experimental procedure or concept adequately. Such identification is not intended to imply recommendation or endorsement by the National Institute of Standards and Technology, nor is it intended to imply that the entities, materials, or equipment are necessarily the best available for the purpose.

degradation may produce an unreliable reading that will likely worsen over time and eventually fail completely. Regular calibration can remedy this only to some extent. Secondly, optical mass flow meters often require a redirection of the flow to achieve the direct line of sight they require. This can include a change in the geometry of the powder's passage, and will create variations in head loss and in turn alter the flow. This intrusive nature should be avoided if possible. There is also some concern of an optical-based system exposed to airborne contaminants that may impede the light used for flow monitoring.

The work described in [14] develops a control algorithm that allows for real-time control of the material delivery rate. The work is promising in addressing the demand to make DED a reliable repeatable process. While the research conducted used an infrared emitter-detector pair to monitor the flow leaving the machine's nozzles (see Fig. 1), effectively guiding the modeling parameters, the apparatus is unable to be used in-situ because of extreme conditions in the build chamber. Therefore, the control system must rely on the assumption that the LENS powder delivery system, set by adjusting the rotational speed of a mechanism that includes an auger and powder carrying wheel, provides a consistent and repeatable mass flow rate. Furthermore, since the actual mass flow rate is not measured simultaneously with the IR data, an accurate quantitative relationship between actual flow rate and the IR signal is difficult to derive. It is clear from Fig. 1 that the IR sensor data does not precisely follow the set powder feeder setting. Whether this is representative of the actual flow rate or an artifact created by the IR sensor cannot be deciphered without knowledge of the real flow rate. There is a need for a robust, reliable, non-intrusive, multi-phase mass flow meter capable of providing quantitative information.

The use of acoustic emission (AE) sensors to monitor powder mass flow offers a promising alternative method to optical sensing. AE has already proven to be a useful and robust tool throughout a multitude of different industries [15–20]. This method is non-intrusive and is unaffected by the presence of dust as the apparatus is placed in an enclosed housing. Furthermore, since AE generated within a material, manifesting as elastic waves on the surface of the material, cover a relatively high frequency range (typically from 20 kHz to 1 MHz), lower frequency machine vibrations will not hinder the device's performance [21].

Theoretical and experimental work characterizing the relationship between AE and normally impinging particles (Fig. 2: left-hand side) has been done, and while this configuration does eliminate the added complexity of oblique particle impact (Fig. 2: right-hand side), it cannot be used for in situ monitoring [22–26]. Although this previous body of work illustrates the capabilities of AE in monitoring particle impingement, a precursor to flow rate monitoring, it does not extend the practical implementation into an industrial practice. In fact, Droubi et al. [24] state the need for experimentation with the 'target plate' placed in a flow loop, and suggest this as the next step in implementation of an AE flow monitoring system in an industrial practice.

It is generally accepted that AE is related to the kinetic energy ($\frac{1}{2}mv^2$) of the impacting particles, and this has been shown experimentally in [22–26] where the size of the particles (i.e., mass assuming constant material density) impacting the 'target plate' is found to correlate well with AE. In [22], [24], and [26] AE is shown to correlate closely with the

velocity of the particles. Though this fact alone translates to increased complexity for AE sensing with the often-changing feedstock type (i.e., changing particle size distribution, density) in the LENS process, there are other factors to consider. These include the plasticity of impact, surface characteristics of particle and target plate, and changes in attenuation of the medium. Now if the conditions present in LENS's two-phase fluid flow are considered, one must additionally account for the velocity profile of the flow, the angle of incidence, surface condition of the channel, frequency of particle impact, and any potential change in particle size as a function of distance from the center of the flow. This list is by no means exhaustive, but should serve as evidence of the convoluted nature of the relationship between AE and the flowing metal powder.

Substantial effort would be needed to simply quantify these unknowns, and much more to theorize how each contributes to the transduced AE signal. Therefore, an easily calibrated system is preferred. The calibration process will account for an aggregate of the particle metrics (size, density, velocity) in addition to other difficult-to-control process variables (e.g., ambient temperature that changes the carrying gas dynamics and how AE attenuates, localized changes in the particle size distribution of the feedstock, surface condition and morphology of particles). Because this system is easily calibrated, the effects from using a new material or different particle size distribution can be accounted for.

As described earlier, RMS is the metric of choice for generating the time series. The reason for this choice is two-fold. Primarily, RMS can be used to simplify the raw AE signal produced by particle impact while maintaining enough fidelity of the original signal [24]. Secondly, the RMS of the waveform has proven useful in measuring multi-phase flow [27,28]. Arrington was able to use the RMS of the AE signal to monitor the mass flow rate of various types of metal powder in a gas stream [27]. Hii et al. were able to use both the RMS and energy of the AE waveform to monitor a two-phase flow consisting of oil and sand in a pipeline [28].

This paper documents the work done to create an AE mass flow meter for the LENS process. The work includes the creation of a mathematical model to describe the actual mass flow rate as a function of the RMS of the AE signal and an apparatus that allows in situ AE sensing. This mathematical model can be calibrated for different materials, sensors, and conditions of operations and still prove effective. The end goal of this work is to provide a tool that utilizes acoustic emission data to provide an operator with an accurate measurement of the mass flow rate of the powder traveling through the machine's nozzles, that will enable comparison of the actual mass flow rate (measured using AE) with the desired flow rate.

2. Experimental setup

The majority of published research work as well as industrial practice assumes the mass flow rate of powder to be constant at each powder feeder setting. Optically based sensing methods previously described rely on this notion. The following section describes how the actual real-time flow can be measured and how it is used to extract the relationship between the AE signal and the flow rate. A commercially available 316 L stainless steel gas atomized powder (-140 +325 mesh; log-normal size distribution) is used in all the reported

experimental data unless noted otherwise. A sample of the powder is shown in an SEM micrograph in Fig. 3, and as shown the particles are generally spherical with smaller satellite particles attached (i.e., cohesion of particles during the solidification in the atomization process).

2.1. Mass flow rate measurement

A system was designed and fabricated to simultaneously measure the mass flow rates of metal powder and the AE created by these particles obliquely impinging the surface of a cylindrical channel. The schematic representation of the system is shown in Fig. 4. It consists of a powder feeder that conveys metal powder carried by an inert gas to the LENS processes' deposition head. Prior to reaching the head the powder-gas mixture travels through the AE sensor mount. Upon exiting the head's four nozzles the two-phase flow travels through polyethylene tubing to powder reservoirs resting on a scale. The reservoirs are vented using 5-micron sintered brass filters that allow the carrying gas to escape while capturing the metal powder so that it can be weighed as a function of time. The scale, has a resolution of 0.01 g and connects to a personal computer running LabVIEW that acquires the scale's weight data at a frequency of 10 Hz. Data synchronization of the signals of the scale and time occurs via a LabVIEW time loop, allowing accurate recorded times of the scale's weights. The difference in weight divided by the difference in time provides a representation of the actual mass flow rate traveling through the nozzles. The scale's combined uncertainty is shown in Table 1 along with each of the contributors. The calculation of the total combined standard uncertainty is the root of the sum of the squares of each of the contributing factors (provided by the scale manufacturer) as shown in Table 1. While the acquisition rate is only 10 Hz, the timing used by the LabVIEW software has a resolution of1 ms and, therefore, its contribution to the measurement uncertainty is negligible in comparison to the scale's contribution. The powder from each nozzle flows into a separate powder reservoir, so while this system only uses one scale, and therefore measures the combined mass flow rate of the four nozzles, each reservoir can be monitored individually.

Since the powder particles are in motion prior to being weighed, the contribution to the force measured from their change in momentum must be considered. To test this effect, the following procedure was followed. The difference in the mass of the reservoirs before and after three tests (when flow rate is at zero) were compared with the time integrated mass flow rate. This difference provides a quantification of the effect of momentum on the scale's mass data. The percent difference between the two methods for all three tests were all less than 0.05%, consequently the momentum effect is assumed negligible.

2.2. Acoustic emission sensor description

The function of the AE sensor is to generate a signal that is proportional to the mass-flow rate. As mentioned in the introduction, the adopted AE is a piezo-electric transducer. The sensor must not disturb the mass-flow of the powder; this means that the sensor must be integrated into the powder feed line. A consequence of this fact implies that the sensor must be positioned parallel to the flow. A commercially available 375 kHz peak frequency AE sensor with a 35 dB integrated preamp is chosen. The sensor operates in a frequency range

of 250 kHz–700 kHz providing a sufficient response in the standard to high frequency range. Fig. 5 shows the actual design adopted for the AE sensor mount.

The primary design specification for the sensor mounting is to be nonintrusive. The stainless-steel mount has a bore of the same diameter than the polyethylene tubing of the feeder system securing a straight trajectory of the flow. The design of the connection between the plastic tube and the bore of the mount is done so it provides a smooth transition avoiding any cavities or alterations to the cross-sectional area. The sensor floor is in close proximity to the flow channel ensuring that the waves travel through with the least attenuation possible. This distance (i.e., sensor floor to cylindrical channel) was found to provide an optimal signal-to-noise ratio at around 3mm using more than five other designs and empirical trial and error. An enclosure, not shown in Fig. 5, is used to apply a constant force to the top of the AE sensor and to minimize contamination and noise. To improve noise isolation from outside sources a neoprene rubber layer is placed between the enclosure and the sensor. Vallen's AMSY-6 AE with a 40 MHz sampling rate at 18 bit dynamic range is used to record the AE data.

2.3. Signal processing

A series of signal processing steps are conducted in order to extract a useful relationship between the data acquired from the scale and the RMS of the AE signal. As mentioned in the introduction the goal of this research work is to produce a sensor that can provide an accurate measurement of the mass flow rate of the metal that is sent to the LENS nozzles. This data can then be compared with the desired flow rate (i.e., set flow rate) and provides a user feedback to control the process of powder deposition. It is theorized that the RMS of the AE signal can be used to quantitatively measure the mass flow rate. If all other variables affecting AE are assumed constant which is reasonable in this case, this term, $\dot{m}_{AE}$, will be a function the RMS of the AE signal and an array of calibration coefficients or model parameters (β). This AE measured flow rate, $\dot{m}_{AE}$, should be equal to the flow rate measured by the scale, $\dot{m}_S$.

$$\dot{m}_{AE} = f(RMS, \beta) = \dot{m}_S . \quad (1)$$

2.3.1. Raw data processing—The initial step in the raw data processing is a reduction of the noise in the scale's data. This noise is attributed to a combination of electronic noise and the impacts of particles with the reservoir's internal walls as well as already settled powder which create impulse-like features in the signal. In order to smooth these spikes while avoiding substantial biasing of the data, a digital filter utilizing a localized least-squares is used. This filter, known as a Savitzky-Golay filter [29], uses neighboring data points, both before and after the point of interest, to fit a polynomial function. In this case, the window size was found to be optimal at 231 data points with a 3rd order polynomial. In Fig. 6 the raw, unfiltered scale data is juxtaposed with the smoothed data. Next, so that the two data sets can be compared at the same, discrete points in time, the sampling frequency of one data set, is adjusted to match the other. The scale's sampling frequency is chosen

since it is a user-specified constant as compared to the variable, threshold-driven sampling of the AE. The AE data is resampled using a linear interpolation.

2.3.2. Time domain alignment—The next problem to solve is the fact that AE data and the scale data are the output of two separate sensors and hence there is not a common reference point in time that connects the two time-series. To find the necessary time shift or lag(τ), the two signals are cross-correlated, which is defined by

$$R_{xh}(\tau) = \int_{-\infty}^{\infty} x(t)h(t+\tau)dt \quad (2)$$

This produces both cross-correlation values ($R_{xh}(\tau)$) and the lag (τ) at which the values were found. Identifying the lag shift at which the cross-correlation was at a maximum value provides the optimal lag shift. This is illustrated in Fig. 7 while the comparison of both the aligned and unaligned scale signals ($\dot{m}_s$) with the RMS of the AE signal is shown in Fig. 8.

2.3.3. Polynomial regression—Due to the complexity of the relationship between the oblique impact of a plurality of metals particles and the AE generated a simplistic approach is taken. The conversion of the output of the AE sensor from RMS to mass flow is achieved through a multiple linear regression method. The scalar dependent variable, mass flow rate (y_i), is fit to the regressor, RMS of AE signal (x^i), using an ordinary least squares estimation. The sum of the squared residuals,

$$E = \sum_{N}^{i=0} \left[y_i - \left(\beta_i x^i \right) \right]^2, \quad (3)$$

is a measure of the error between the regression model and the empirical data. The fit of the polynomial model is optimal when this error is minimized. By setting the gradient equal to zero,

$$\frac{\partial E}{\partial \beta_i} = 0, \quad (4)$$

the minima can be found and therefore the optimal model parameters or coefficients (β_i) can be selected. These parameters will be a function of the many variables mentioned in Section 1 (e.g., particle size distribution, material density, angle of incidence).

2.3.4. Pearson's correlation coefficient—Finally, to compare the goodness of fit for the developed models, Pearson's correlation coefficient is used. Pearson's correlation coefficient, also known as the sample correlation coefficient, *r*, is defined as

$$r = \frac{\sum_i (x_i - \bar{x})(y_i - \bar{y})}{\left(\sqrt{\sum_i (x_i - \bar{x})^2}\right)\left(\sqrt{\sum_i (y_i - \bar{y})^2}\right)}, \quad (5)$$

where x_i and y_i are data points in each of the respective signals (i.e., scale data and RMS of AE), and $\bar{x}$ and $\bar{y}$ are the mean values of the signals. The closer r is to 1 the more positively correlated the two signals are. This provides a metric to compare each of the model's parameters including the order of the polynomial used in the regression and the window size of the Savitzky-Golay filter. This signal processing scheme is used to extract the estimated effects (i.e., regression coefficients) unique to each material and PSD, and therefore should be conducted after changing any process parameter that may alter the AE signal.

3. Results and discussion

3.1. Setting model parameters

The signal processing scheme detailed is conducted on data taken from flowing 316 L stainless steel gas atomized powder through the LENS system. Initially, to extract the optimal model parameters (β_i), the LENS's powder delivery system is operated at a rate of 6 rpm (i.e., the rotational speed of the powder feeder's auger/wheel) then increased to 7 rpm after about 50 s. The resulting model parameters or regression coefficients are shown in Table 2, and the mass flow rate measured using the scale and the AE sensor are shown in Fig. 9. The filter used and the respective sample correlation coefficients are listed on the right-hand side. The mass flow rate measured using the AE system ($\dot{m}_{AE}$) proves to follow the actual mass flow rate closely with the exception of the high frequency perturbations in the scales' data. The benefit of using a relatively wide sample window for the Savitzky-Golay filter is obvious with a sample correlation coefficient of 0.959 compared to 0.827 when comparing the unfiltered data. A sample window of 191 (i.e., 19.1 s) was found to be optimal with wider windows leading to detrimental correlation values.

3.2. Experimental evaluation of the AE mass flow meter

Using the model parameters identified in the previous section, the system is tested through a range of power feeder settings. As shown on Fig. 10, the powder feeder is held for 80 s at various settings ranging from 4 rpm to 8 rpm in both increasing and decreasing fashions to test for hysteresis. These settings represent the range of the powder feed rate used in normal operation of this powder fed DED process. Not only is there no hysteresis between the signals, but the signals have a sample correlation coefficient of 0.985 signifying a strong correlation. It's interesting to point out that the raw signals maintain the correlation over a rather dynamic range (from about 5 g/min to about 14 g/min). Even when the powder feeder's setting is changed by 200% and the actual flow rate more than doubles, the correlation is maintained.

Fig. 10 also illustrates two potential issues with the consistency of the delivery rate. Seen throughout the test, but particularly evident in the 4, 7 and the first of the two 5 rpm test segments, a significant fluctuation (up to 10%) in the mass flow rate is present. Each of the

80 s test segments uses a constant powder feeder setting, but the measured mass flow rate (both $\dot{m}_s$ and $\dot{m}_{AE}$) deviates from steady state. This is expected during insipient flow or immediately following a change in the powder feeder's setting when the flow is not fully developed, but in this case these deviations are seen more than 30 s after a change in the settings. Secondly, specific powder feeder settings may not always produce the same actual mass flow rate. This is illustrated in a comparison of the two 4 rpm settings in Fig. 10. The average of each of the two sections vary by more than 13% (5.24 g/min compared to 6.05 g/min for the second 4 rpm segment). While this may be due to an insufficient amount of time for the flow to reach steady state, it warrants further investigation. Both of these characteristics can be seen in Fig. 1 suggesting this may not be an isolated event. To the authors' knowledge this has not been documented prior to this work and is to be further inspected. Aside from these fluctuations in the flow rate, the newly developed AE mass flow monitoring systems proves itself capable of accurately measuring the flow of this 316 L stainless steel powder throughout both a wide range and abrupt changes in the rate of flow.

3.3. AE mass flow monitoring of commercially pure titanium

The equivalent signal processing scheme was conducted on a commercially pure titanium (Cp-Ti) powder to evaluate whether the system is capable of monitoring other metal powders. The powder has a similar particle size distribution as the 316 L powder in Fig. 3. As illustrated in Fig. 11, $\dot{m}_s$ and $\dot{m}_{AE}$ have a sample correlation coefficient of 0.967 indicating a high correlation. There seems to be a slight error in the lag shifting, but otherwise the AE mass flow meter system proves to be capable of accurately monitoring the flow rate of this material. The material produces different model parameters as shown in Fig. 11, which are indirectly accounting for the change in material. Other materials should be evaluated, but since the kinetic energy ($\frac{1}{2}mv^2$) is the primary factor in the production of AE, mass flow rates of powder particles with similar velocities and masses should be quantifiable with this system.

4. Conclusions

A novel mass flow monitoring system and calibration method using acoustic emission for powder DED was developed and tested. The system can accurately measure a wide range of mass flow rates of metal powders in a powder fed directed energy deposition process. Prior attempts at mass flow monitoring of metal powders have lacked the essential calibration process or were incapable of being used in situ effectively limiting their utility. The aforementioned mass flow monitoring system excels in both of these pursuits.

The calibration process utilizes a high precision scale connected to a data acquisition system to measure the actual mass flow rate of metal powder as a function of time. Prior to the flow reaching the scale, the powder transmission line is connected to the AE sensor so that both the scale and the AE sensor can record in regards to the flow simultaneously. After signal conditioning, the two can be directly compared providing a means for model parameters to be derived. These para-meters will be based off any sources of variability in terms of the AE produced. These sources include changes in particle size distribution, density, morphology, and angle of incidence.

While the relationship between AE and particle impact has previously been analytically modeled, the increased complexity due to the oblique angle of impact and distribution of particle sizes amongst other variables, makes application quite difficult. The calibration used in this work allows these variables to be accounted for without needing to be quantified. While only several materials have been tested using this system and only two reported here, the system seems to be capable of evaluating a wide range of materials.

A promising application of this system is real time monitoring of the mass flow rate of powder through individual nozzles in the deposition head. This would easily identify clogs or inconsistencies in flow through individual nozzles. However, the extreme environment and spacing constraints do not allow direct attachment of the sensors to the nozzles or powder flow channels. For real time monitoring of individual nozzles using AE sensors to be possible, ‘waveguides’ have to be implemented into the system. A waveguide would act as a medium for certain modes of waves to travel that an AE sensor can measure. Research work is currently underway investigating the plausibility of using waveguides for the powder blown DED process.

Significant flow variability has been documented illustrating the utility for an in situ mass flow meter. In both steady-state and transient flow scenarios variability on the order of 10% was recorded. Further work shall focus on characterizing the fluctuations in the mass flow rate over various temporal scales and for different materials. These scales should include fluctuations that take place over several seconds, 15 s to 60 s, 60 s to 1 h., and potentially up to days to characterize long-term deviations from expected flow rates. The information provided by the system is currently being used as an input to research devoted to the optimization of the LENS manufacturing process. Powder flow rate being one of the three primary process parameters for LENS, is being used alongside travel speed and laser power to identify optimal operating conditions. From this work, it seems the rate of powder deliver can be accurately measured in situ allowing future control schemes to be developed.

Acknowledgments

The authors would like to express their gratitude to the NIST Measurement Science for Additive Manufacturing (MSAM) program for the opportunity to perform this research. The efforts put forth were performed under the following financial assistance award [70NANB 13Hl 94] from the U.S. Department of Commerce, National Institute of Standards and Technology. The views expressed do not necessarily reflect the official policies of NIST; nor does mention by trade names, commercial practices, or organizations imply endorsement of the U.S. Government.

Abbreviations:

AE	acoustic emission
DED	directed energy deposition
LENS	laser engineered net shaping
RMS	root mean square
AM	additive manufacturing

References

[1]. Kumar A, Paul CP, Pathak AK, Bhargava P, Kukreja LM, A finer modeling approach for numerically predicting single track geometry in two dimensions during laser rapid manufacturing, Opt. Laser Technol 44 (3) (2012) 555–565.

[2]. Kobryn PA, Moore EH, Semiatin SL, The effect of laser power and traverse speed on microstructure, porosity, and build height in laser-deposited Ti-6Al-4V, Scr. Mater 43 (4) (2000) 299–305.

[3]. Neela V, De A, Three-dimensional heat transfer analysis of LENSTM process using finite element method, Int. J. of Adv. Manuf. Technol 45 (2009) 935–943.

[4]. Ferguson JB, Schultz BF, Moghadam AD, Rohatgi PK, Semi-empirical model of deposit size and porosity in 420 stainless steel and 4140 steel using laser engineered net shaping, J. Manuf. Process 19 (2015) 163–170.

[5]. Amine T, Newkirk JW, Liou F, An investigation of the effect of direct metal deposition parameters on the characteristics of the deposited layers, Case Stud. Therm. Eng 3 (2014) 21–34.

[6]. Griffith M, Keicher D, Atwood C, Romero J, Smugeresky J, Harwell L, Greene D, Freeform fabrication of metallic components using laser engineered net shaping, Solid Freeform Fabr. Proc (1996) 125–132.

[7]. Pityana S, Mahamood RM, Akinlabi ET, Shukla M, Gas flow rate and powder flow rate effect on properties of laser metal deposited Ti6Al4V, Int. MultiConf. Eng. Comput. Sci 2 (2013) 848–851.

[8]. Majumdar JD, Pinkertona A, Liub Z, Mannac I, Lia L, Microstructure characterisation and process optimization of laser assisted rapid fabrication of 316L stainless steel, Appl. Surf. Sci 247 (1) (2005) 320–327.

[9]. Wang L, Pratt P, Felicelli SD, El Kadiri H, Berry JT, Wang PT, Horstemeyer MF, Pore formation in laser-assisted powder deposition process, J. Manuf. Sci. Eng 131 (5) (2009) 389–396.

[10]. Dongming H, Kovacevic R, Sensing, modeling and control for laser-based additive manufacturing, Int. J. Mach. Tools Manuf 43 (1) (2003) 51–60.

[11]. Hu XD, Kong FZ, Yao JH, Development of monitoring and control system for laser remanufacturing, Appl. Mech. Mater 44 (2011) 81–85.

[12]. Xing F, Liu W, Zhang K, Shang X, Wang T, Intelligent metal powder laser forming system, knowledge enterprise: intell. strategies in product, Des. Manuf. Manage 207 (2006) 525–535.

[13]. Lin J, Steen W, Design characteristics and development of a nozzle for coaxial laser cladding, J. Laser Appl 10 (2) (1998) 55–63.

[14]. Tang L, Ruan J, Landers RG, Liou F, Variable powder flow rate control in laser metal deposition processes, J. Manuf. Sci. Eng 130 (4) (2008) 041016.

[15]. Le Moal G, Rabaté P, Moraru G, Véron P, Douilly M, A robust method for drilling monitoring using acoustic emission, Proc. of the 9th Int. Conf. on High Speed Mach. – HSM, (2012).

[16]. Quan Y, Zhou M, Luo Z, On-line robust identification of tool-wear via multi-sensor neural-network fusion, Eng. Appl. Artif. Intell 11 (6) (1998) 717–722.

[17]. Howells E, Norton ET, Detection of partial discharges in transformers using acoustic emission techniques, Ieee Trans. Power Appar. Syst 97 (5) (1978) 1538–1549.

[18]. Antonaci P, Bocca P, Masera D, Fatigue crack propagation monitoring by acoustic emission signal analysis, Eng. Fract. Mech 81 (2012) 26–32.

[19]. Yan J, Heng-hu Y, Hong Y, Feng Z, Zhen L, Ping W, Yan Y, Nondestructive detection of valves using acoustic emission technique, Adv. Mater. Sci. Eng. Int. J 2015 (2015), 10.1155/2015/749371.

[20]. Boyd JWR, Varley J, The uses of passive measurement of acoustic emissions from chemical engineering processes, Chem. Eng. Sci 56 (5) (2001) 1749–1767.

[21]. Al-Lababidi S, Mba D, Addali A, Upstream multiphase flow assurance monitoring using acoustic emission, in: Sikorski Wojciech (Ed.), Acoustic Emission, InTech, Rijeka, Croatia, 2012, pp. 217–250.

[22]. Buttle DJ, Scruby CB, Characterization of particle impact by quantitative acoustic emission, Wear 137 (1) (1990) 63–90.

[23]. Boschetto A, Quadrini F, Powder size measurement by acoustic emission, Measurement 44 (1) (2011) 290–297.

[24]. Droubi MG, Reuben RL, White G, Statistical distribution models for monitoring acoustic emission (AE) energy of abrasive particle impacts on carbon steel, Mech. Syst. Signal Process 30 (2012) 356–372.

[25]. Ivantsiv V, Spelt JK, Papini M, Mass flow rate measurement in abrasive jets using acoustic emission, Meas. Sci. Technol 20 (9) (2009) 095402.

[26]. Faisal NH, Ahmed R, Reuben RL, Allcock B, AE monitoring and analysis of HVOF thermal spraying process, J. Therm. Spray Technol 20 (5) (2011) 1071–1084.

[27]. Arrington M, The use of acoustic emission instrumentation to monitor powder flows, NDT Int. 14 (1) (1981) 3–8.

[28]. Hii NC, Tan CK, Wilcox SJ, Chong ZS, An investigation of the generation of acoustic emission from the flow of particulate solids in pipelines, Powder Technol. 243 (2013) 120–129.

[29]. Savitzky A, Golay MJE, Smoothing and differentiation of data by simplified least squares procedures, Anal. Chem 36 (8) (1964) 1627–1639.

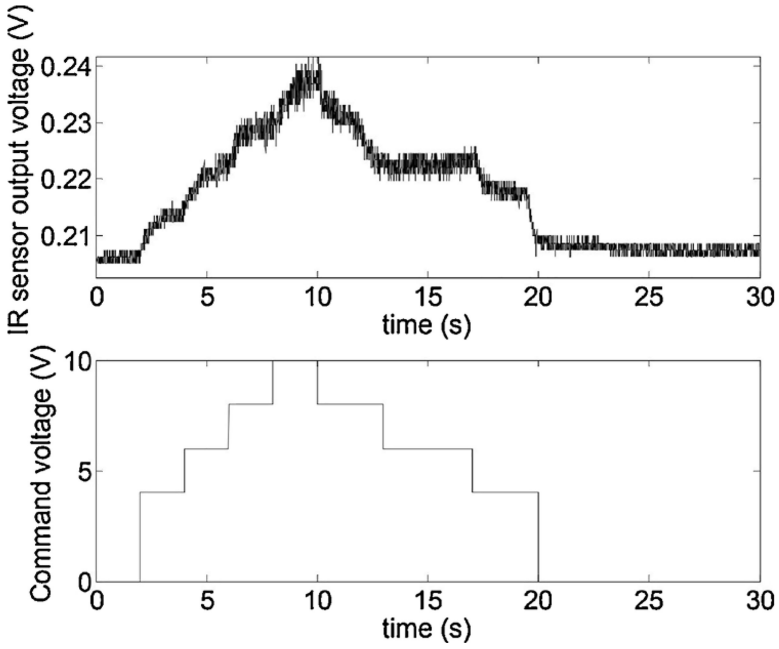

Fig. 1.

Infrared sensor feedback as a function of powder delivery system command voltages [14].

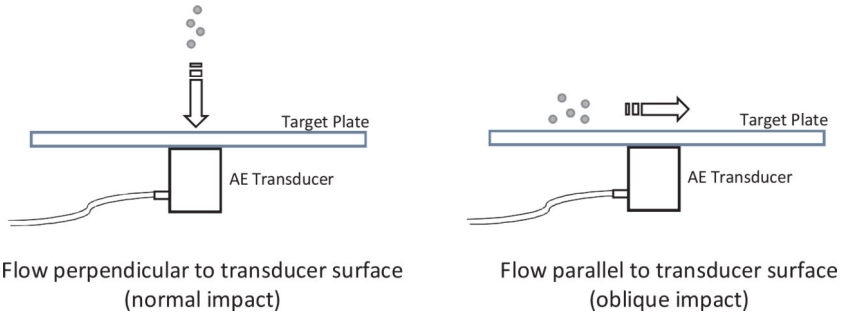

Fig. 2.

Schematic comparing normal versus oblique particle impact with respect to AE sensor.

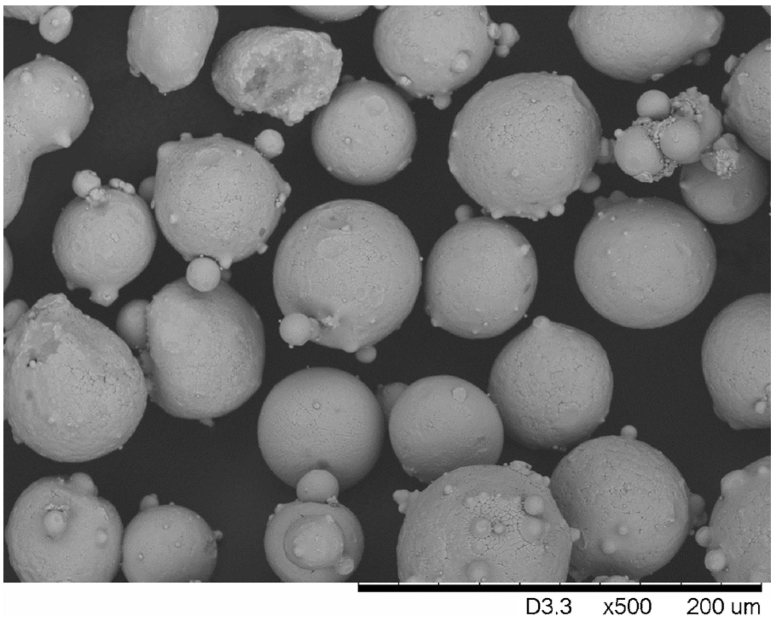

Fig. 3.
SEM micrograph of virgin 316 L stainless steel powder.

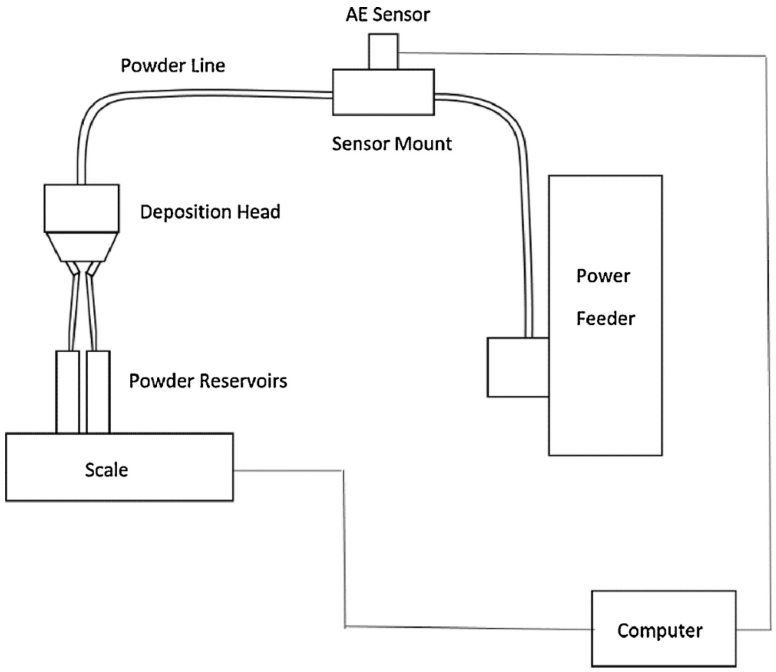

Fig. 4.
Schematic of in-situ flow monitoring using AE sensor and scale simultaneously.

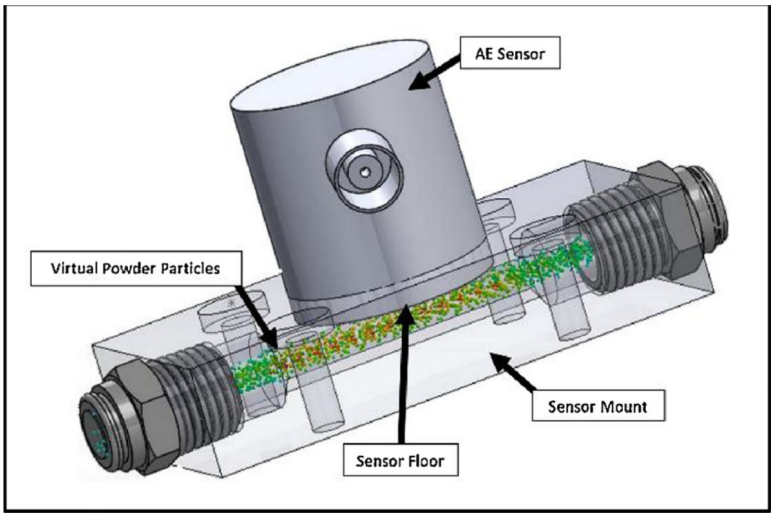

Fig. 5.
Powder sensor mount and sensor with virtual particles to visualize powder flow.

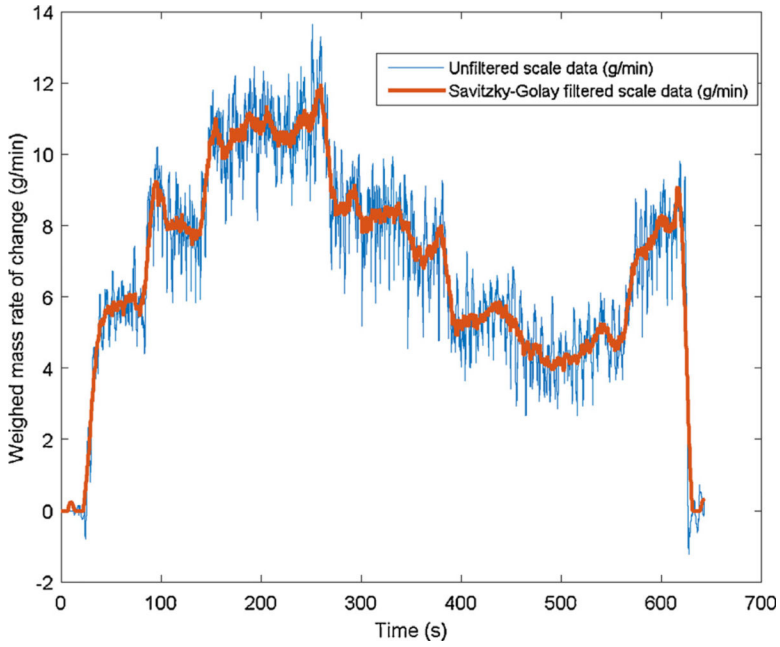

Fig. 6.
Savitzky-Golay filtered scale data compared to raw data.

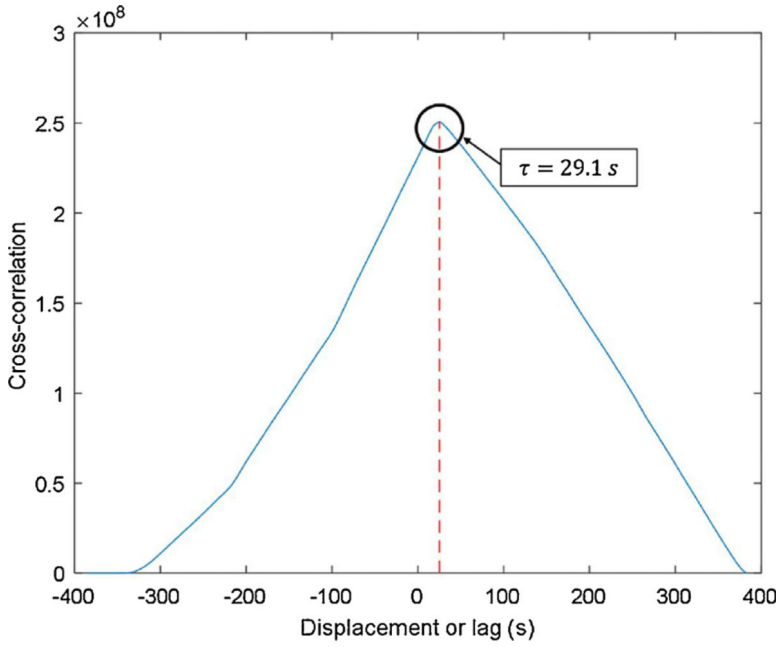

Fig. 7.
Cross-correlation as a function of time lag.

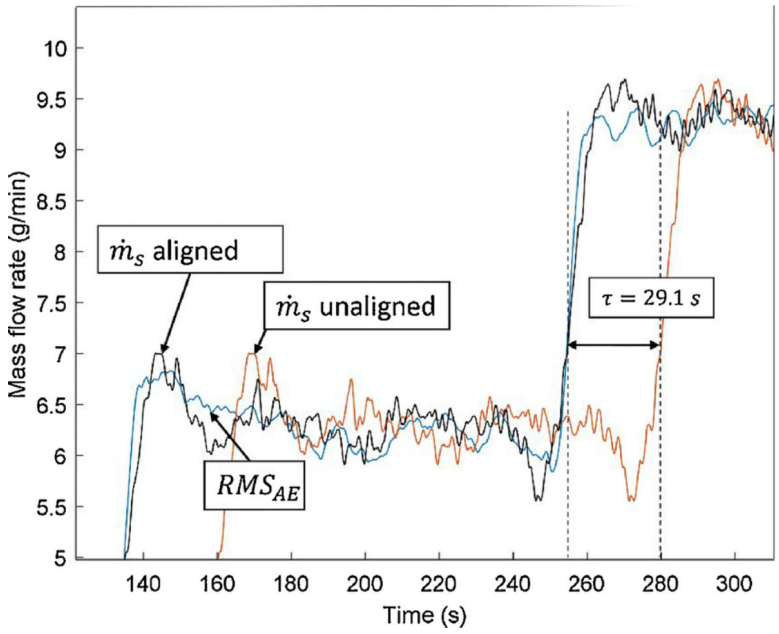

Fig. 8.

Comparison of both aligned and unaligned scale mass flow rates ($\dot{m}_s$) with the RMS of the AE signal.

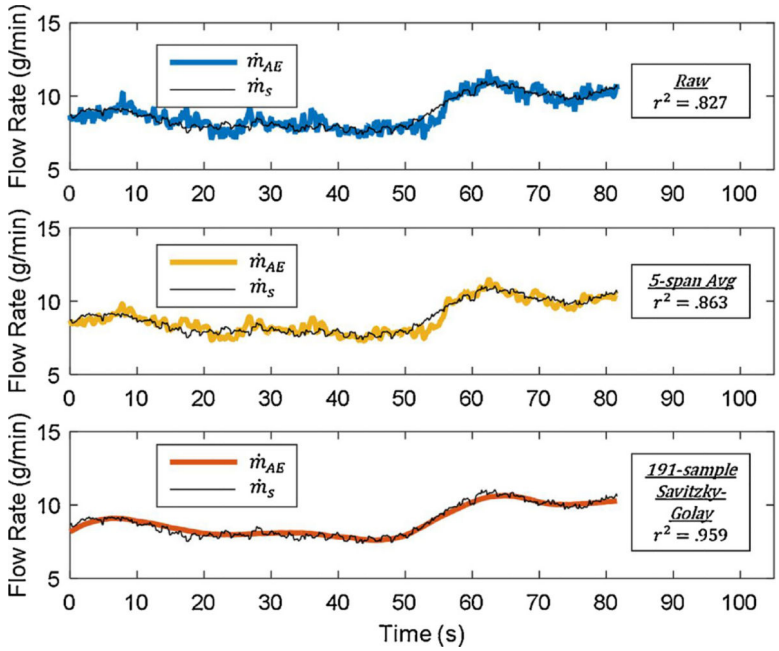

Fig. 9.

Comparison of various smoothing filters and the affect they have on the sample. correlation coefficient between the actual mass flow rate ($\dot{m}_s$)and the AE measured mass flow rate ($\dot{m}_{AE}$).

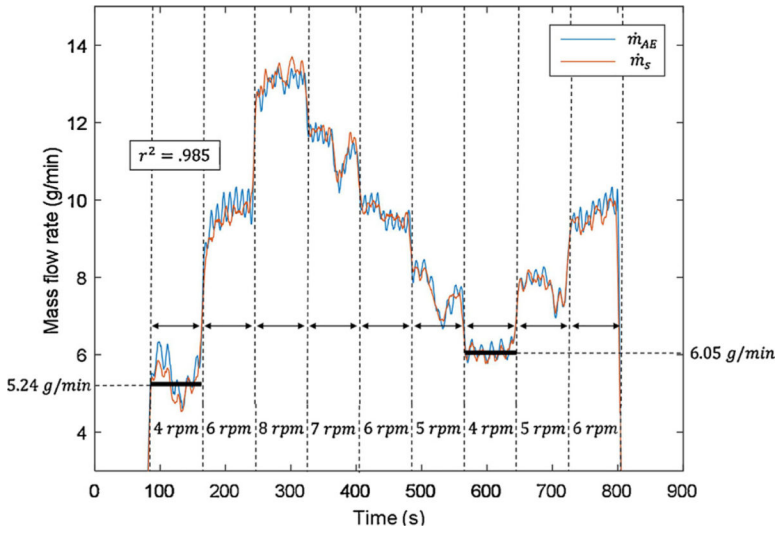

Fig. 10.

Correlation between the mass flow data extracted from the scale readings and the AE sensor after the procedures described in Section 2 are applied.

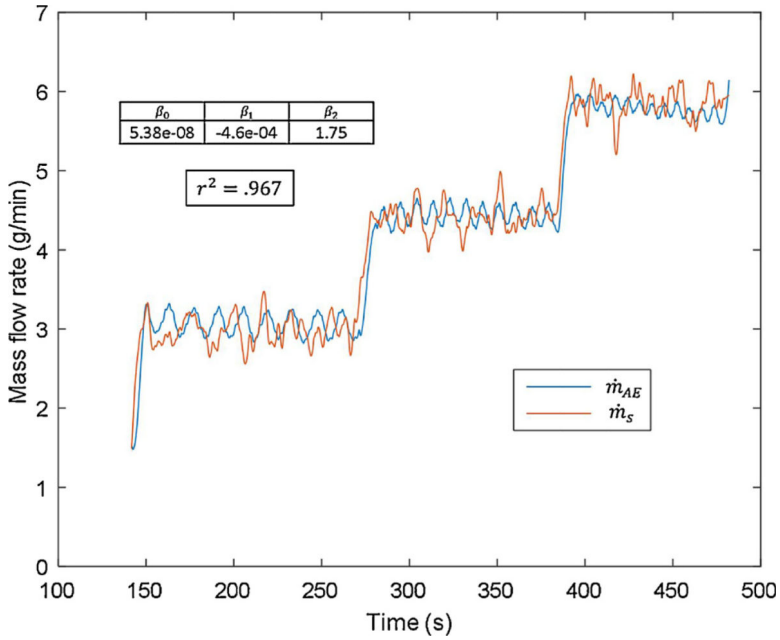

Fig. 11.

Commercially pure titanium (Cp-Ti) powder model parameters and mass flow rates measured by AE system and scale.

Table 1

Mass Scale Uncertainty.

Resolution	0.01 g	$u^2(x_1)$
Repeatability	0.01 g	$u^2(x_2)$
Linearity Deviation	0.02 g	$u^2(x_3)$
Sensitivity Temperature Drift (assuming 5 K maximum temperature change)	1.5×10^{-5} g	$u^2(x_4)$
Combined Standard Uncertainty of Scale	0.02 g	$U_c(y) = \sqrt{\sum_{i=1}^{n} \left[\frac{\partial f}{\partial x_i}\right]^2 u^2(x_i)}$

Table 2

Derived model parameters for 316 L stainless steel gas atomized powder.

β_0	β_1	β_2
3.41e-09	−1.50e-04	3.89